1

Defects in Germanium

Justin R. Weber, Anderson Janotti, and Chris G. Van de Walle

1.1

Introduction

Many properties of solids are strongly affected by the presence of defects or impurities. In semiconductors, impurities are routinely incorporated in small quantities as a means of controlling the electrical conductivity. This practice, referred to as doping, is at the heart of modern solid-state device design, where *p*-*n* junctions are used in a myriad of different applications such as diodes, transistors, light emitters, and solar cells. A *p*-*n* junction is an interface between two semiconductor regions of different conductivity type: *p*-type and *n*-type. *n*-type semiconductors contain impurities referred to as donors, which contribute electrons to the empty conduction-band states of the semiconductor that lead to *n*-type conductivity. In a *p*-type semiconductor, the presence of impurities called acceptors causes electrons to be removed from the filled valence-band states. These removed electrons leave behind mobile charged electronic vacancies in the valence band (referred to as holes), which induce *p*-type conductivity.

In addition to intentionally incorporated impurities, native point defects are also present. These are defects that are intrinsic to a given material, such as vacancies (missing atoms), self-interstitials (additional atoms), or antisites (a cation sitting on an anion site or vice versa in a compound semiconductor). Such native point defects are typically electrically active, and can lead to compensation, that is, a reduction in the conductivity that one aims to achieve by incorporating dopant impurities. Native point defects are involved in self-diffusion [1], but also play a critical role in dopant diffusion, because the motion of impurities is typically assisted by vacancies or self-interstitials [2–5]. Point defects may also act as carrier traps or be involved in degradation.

It is therefore crucial to understand the nature and origin of point defects in order to control their formation and concentration. This is particularly important because germanium has emerged as a promising material for use in the channel of novel complementary metal-oxide Semiconductor (CMOS) devices. Compared to silicon CMOS, germanium offers higher channel mobilities and lower voltage operation due to its significantly smaller band gap. However, problems exist,

Photonics and Electronics with Germanium, First Edition. Edited by Kazumi Wada and Lionel C. Kimerling.

Table 1.1 Bulk properties of silicon and germanium.

Property	Silicon	Germanium
Band gap (eV)[a)]	1.15	0.75
Electron mobility (cm^2 $(V \cdot s)^{-1}$)[b)]	1500	3900
Hole mobility (cm^2 $(V \cdot s)^{-1}$)[b)]	470	1900
Electron effective mass (m_e)[c)]	1.08	0.55
Hole effective mass (m_e)[c)]	0.56	0.37
Static dielectric constant[b)]	11.7	16
Lattice constant (Å)[a)]	5.43	5.66
Bulk modulus (GPa)[a)]	98	75
Cohesive energy (eV/atom)[a)]	4.63	3.85

a) $T = 0\,K$ data from Ref. [6].
b) $T = 300\,K$ data from Ref. [7].
c) Density-of-states effective mass ($T = 300\,K$) from Ref. [8].

particularly in n-channel MOS field-effect transistors (FETs), which are likely caused by the presence of defects near the semiconductor/dielectric interface, such as germanium dangling bonds (DBs).

Throughout this chapter, we will occasionally compare results for germanium with those for silicon. Such comparisons are meaningful not only because germanium is frequently integrated with silicon in devices, but also because of the similarities between the two semiconductors. Germanium, like silicon, is a semiconductor with the diamond crystal structure. Both are indirect semiconductors with similar properties, as shown in Table 1.1. However, the conduction-band minimum (CBM) in germanium occurs at the L-point in the Brillouin zone, while the CBM occurs near the X-point in silicon. In addition, germanium has a significantly higher hole mobility compared to silicon, making it a desirable choice for a number of applications.

1.2
Methods for Studying Defects and Impurities

1.2.1
Experimental Techniques

A number of experimental techniques exist for studying point defects and impurities.

Electron spin resonance (*ESR*) is one of the most powerful techniques for the study and identification of defects in semiconductors [9]. It provides information about the chemical identity of the atoms in the vicinity of the defect, as well as about the symmetry of the defect. ESR relies on the presence of unpaired electrons. In cases where the stable ground-state configuration of the defect is not paramagnetic, optical excitation can often be used to generate a metastable charge state with a net spin density. Optically detected magnetic resonance (ODMR) is a variant of the technique that can offer additional information about defect-induced levels in the band gap [10]. The ability to directly compare measured hyperfine parameters with calculated values for specific defect configurations allows for an explicit identification of the microscopic structure [11, 12].

Vibrational spectroscopy can be applied to defects or impurities that give rise to local vibrational modes (LVMs), whose frequencies and polarization contain information about the chemical nature of the atoms involved in the bond as well as the bonding environment [13]. Comparisons with calculations [14] can again facilitate the identification of the observed defect and its structure.

Positron annihilation spectroscopy (*PAS*) [15] can be used to identify point defects and measure their concentration, but it is mostly sensitive to negatively charged defects and typically limited to detection of vacancies.

The electronic structure of defects can be studied with electrical techniques such as *temperature-dependent Hall measurements* [16] or *deep-level transient spectroscopy* (*DLTS*) [17]. Optical levels can be observed in *photoluminescence, absorption, or cathodoluminescence experiments*[18].

Finally, we mention *perturbed angular correlation spectroscopy* (*PACS*), which is a type of γ-ray spectroscopy that is used to study hyperfine interactions on probe nuclei introduced into a crystal. Point defects near the probe nuclei modify internal fields, allowing the determination of defect association energies, migration barriers and formation energy differences between defects within a crystal [19, 20]

1.2.2
First-Principles Calculations

Modern first-principles calculations can provide deep insight into the nature of defects and impurities in semiconductors. Owing to a substantial increase in available computational power as well as in the development of novel algorithms, first-principles techniques have achieved an unprecedented level of predictive power, accuracy, and the ability to treat systems with an increasingly large number of atoms. Such methods allow calculating the energetic properties of solids at the microscopic level and the investigation of both the atomic and electronic structure of defects and impurities. As mentioned in Section 1.2.1, first-principles methods allow calculating observables that can be directly compared with experiments, and also quantities that are difficult to extract directly from experiments such as electronic wavefunctions, microscopic charge densities, defect formation energies, and local atomic relaxations.

Most state-of-the-art first-principles (or *ab initio*) calculations for defects and impurities in solids are based on density functional theory (DFT) [21]. DFT seeks to determine the ground-state properties of the many-body electronic system present in solids. DFT in the Kohn–Sham (KS) scheme [22] provides an approximate solution to this problem by formulating it as a single-particle problem in which the electrons move in an effective potential that is composed of the

Coulomb potential due to the atomic nuclei; the classical Hartree potential due to all of the other electrons in the system; and a so-called exchange-correlation potential (V_{XC}), which captures the quantum-mechanical many-body interactions. An exact expression for V_{XC} is not known, but approximations such as the local density approximation (LDA) or generalized gradient approximation (GGA) have been shown to provide very good descriptions of structural properties [23, 24]. Within the LDA, V_{XC} is assumed to depend only on the *local* charge density [22]; the GGA additionally takes local variations of the charge density into account [25, 26]. Within the LDA, V_{XC} is assumed to have the value corresponding to a homogeneous electron gas with a density equal to the local charge density; values for the homogeneous electron gas are obtained with high accuracy from quantum Monte Carlo simulations [27, 28].

DFT with traditional functionals such as the LDA and GGA has been very successful in describing the many properties of molecules and solids, but it has significant shortcomings in its description of electronic band structures, an issue commonly referred to as the band-gap problem, because the band gap of semiconductors and insulators is significantly underestimated. Sometimes this underestimation is so severe that an LDA or GGA calculation actually produces a zero band gap, that is, a metal, which is the case with germanium [29].

A variety of approaches have been proposed to overcome this problem. The most rigorous are based on many-body perturbation theory, the lowest order approximation being the GW approximation [30]. The GW approach is generally regarded as the method of choice for computing excitation spectra of weakly correlated systems, but it still has limitations: it is computationally expensive for calculating the large supercells needed to study defects and impurities, and no practical scheme is currently available for self-consistently calculating energetics and forces (and thus atomic relaxations), rendering it difficult to study cases where large structural relaxations occur [31, 32]. In addition, The GW calculations typically use wave functions calculated with LDA or GGA as input, and problems may arise when defect states do not lie within the DFT-calculated band gap.

A number of approximate correction schemes also exist, the simplest being a "scissors operator," that is, a rigid shift of conduction bands and possibly conduction-band-derived states to bring the fundamental gap in line with the experimental value. More sophisticated approaches based on the extrapolations of certain parameters have been proposed but these introduce additional uncertainties [33]. Pseudopotentials are typically used in conjunction with DFT calculations in order to avoid solving an all-electron problem. The construction of pseudopotentials allows some flexibility in the choice of parameters, and modified pseudopotentials have been successfully implemented for corrections of the DFT band structure [34].

Aside from the band gap, some other features of DFT band structures calculated with LDA or GGA may be inaccurate: semicore states (such as the Ge 3*d* states) are underbound and hence too close to the valence-band states. This error contributing to the band-gap underestimation as *p*-*d* repulsion pushes the valence-band maximum (VBM) upward and closer to the CBM. In the DFT+U scheme, an orbital-dependent potential is applied to the semicore d states. This potential adds an extra Coulomb interaction (U) to such states, and lowers their energetic position on an absolute energy scale. The lowering of the d states shifts the VBM downward (due to p-d coupling) and opens up the band gap. This leads to a partial opening of the band gap, but the band gap is not *fully* corrected as it still suffers from underestimation due to other DFT-inherent causes such as self-interaction errors. Still some improvement in the band structure occurs, and such DFT+U calculations have been applied to defects in germanium [35, 36].

It would be desirable to have a methodology that stays within DFT and retains its capability to efficiently calculate energetics and forces, while improving the band structure. Novel functionals have been developed that have proven successful in achieving these goals. Hybrid functionals essentially mix the standard GGA functional with a certain amount of exact exchange, as would be obtained from the Hartree–Fock method. The two most common implementations of this approach were developed by Perdew, Ernzerhof, and Burke (PBE0) [37–40] and by Heyd, Scuseria, and Ernzerhof (HSE) [41, 42]. Both include 25% Hartree–Fock exact exchange, but the HSE formalism truncates the contributions from exact exchange at a certain length, which allows for more accurate descriptions of metallic systems and also results in a reduction of computational demands.

1.3
Impurities

1.3.1
Shallow Dopants

The most common dopant impurities for silicon and germanium are group-III elements as p-type dopants and group-V elements as n-type dopants. A shallow dopant is characterized by a small ionization energy. For example, arsenic in germanium introduces an extra electron resulting from arsenic having five valence electrons (as opposed to four for germanium). The atomic electronic level corresponding to this arsenic state lies well above the CBM of germanium, and, therefore, the extra electron drops to the bulk CBM of germanium, that is, an extended electronic state. Within that state, the electron is Coulombically attracted to the positive As center, a situation described by hydrogenic effective mass theory. The energy difference between the ground state of this hydrogen-like system (modified by the dielectric constant and the effective mass of the host material) determines the ionization energy. Table 1.2 lists the ionization energies for a number of common dopants in silicon and germanium. Table 1.2 shows that ionization energies are significantly smaller in germanium as compared with silicon, which can be attributed to its larger dielectric constant and smaller effective masses.

Another important characteristic of dopant impurities is their solubility, which determines how easily dopants can be incorporated. Table 1.3 lists the solid solubility limits for some common dopants in silicon and germanium.

Table 1.2 Dopant ionization energies in silicon and germanium.

Dopant impurity	Type	Silicon (meV)	Germanium (meV)
B	*p*-type	45	10
Al	*p*-type	67	10
Ga	*p*-type	72	11
In	*p*-type	160	11
P	*n*-type	45	12
As	*n*-type	54	13
Sb	*n*-type	39	9.6

Source: Data from Ref. [8].

Table 1.3 Dopant solid solubility limits in silicon and germanium.

Dopant impurity	Type	Silicon (10^{20} cm^{-3})	Germanium (10^{20} cm^{-3})
B	*p*-type	6.0	–
Al	*p*-type	0.2	4.0
Ga	*p*-type	0.4	5.0
P	*n*-type	15.0	–
As	*n*-type	19.0	1.9
Sb	*n*-type	0.7	0.1

Source: Data from Ref. [43].

Dopants can be incorporated in a variety of ways. Sometimes this is accomplished during the growth of the material itself; in other cases, in separate treatments. The two most common methods include diffusion and ion implantation. In diffusion techniques, a high concentration of dopant atoms is first introduced onto the surface of the semiconductor by coating the semiconductor surface with a dopant-containing layer, and using elevated temperatures to cause the dopant atoms to diffuse into the semiconductor. In ion implantation, an ion beam bombards the semiconductor substrate, implanting dopants into the material as well as simultaneously damaging the substrate, thus requiring a post-implantation anneal.

In all cases, controlling the spatial distribution of dopants is a challenge. Some applications require an even distribution of dopants throughout the semiconducting material, but state-of-the-art devices typically require precise positioning of dopant atoms over small length scales (on the order of nanometers). This is typically accomplished using ion implantation, followed by a rapid thermal anneal. The diffusivity of many dopants is mediated by native defects in the semiconductor [2, 4]. In the case of germanium, many impurities (such as arsenic) diffuse faster than germanium itself, which may be attributed to both the electrostatic attraction between the impurities and native defects [2, 4]. Figure 1.1 illustrates the higher diffusivity of arsenic compared with self-diffusion in germanium. Other impurities such as boron and silicon diffuse slower than

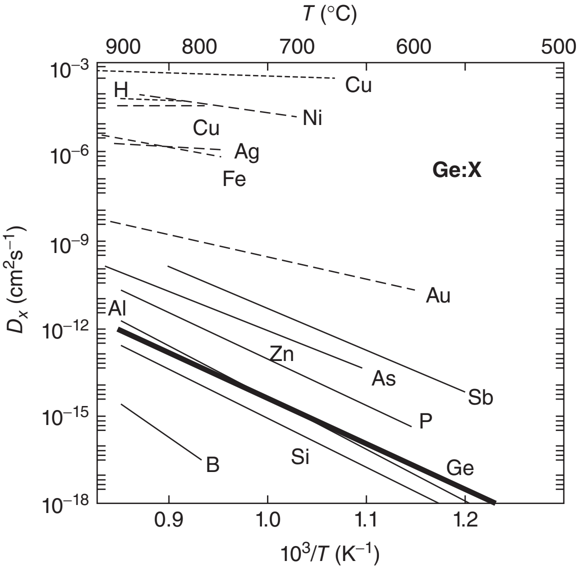

Figure 1.1 Temperature dependence of the diffusion constant of foreign atoms in Ge (thin lines) compared with self-diffusion (thick line). Solid lines represent diffusion data of elements that are mainly dissolved on substitutional lattice sites. Long-dashed lines (– –) indicate hybrid elements, which are mainly dissolved on substitutional sites, but diffuse in an interstitial configuration via the dissociative mechanism. The short-dashed lines (- - - -) indicate elements that are mainly interstitially dissolved. The upper short-dashed line shows the diffusivity deduced for interstitial copper. Figure courtesy of Ref. [2]

the self-diffusion in germanium, which can happen if the impurity atoms are electrostatically repelled from native defects [2].

Impurities can diffuse via substitutional or interstitial sites. Native defects can assist this diffusion through a variety of mechanisms. For example, if a vacancy and substitutional impurity atom are attracted to one another (to minimize local strain, or by electrostatic interaction), they can diffuse to form a complex. This pair can then dissociate and subsequently reform along a different direction, leading to long-range migration [4, 44]. Self-interstitial defects can also assist impurity diffusion. This requires the self-interstitial atom and impurity atom to stay spatially localized and not dissociate. When the self-interstitial (paired with the impurity) diffuses one atomic site, it can create a local lattice distortion that causes the impurity to follow [44]. There are also dissociative mechanisms by which substitutional impurity atoms can diffuse through interstitial sites [44]. Such diffusion involves the creation and destruction of vacancies as the impurity moves from substitutional to interstitial sites. Finally, we mention the *kick-out* mechanism, which is assisted by self-interstitials: the impurity is kicked out of a substitutional site, migrates interstitially, and then rejoins a substitutional site by kicking a bulk lattice atom into an interstitial position. Therefore, in order to fully understand dopant or impurity incorporation (and diffusion), it is clearly essential to study the behavior of native defects.

1.3.2
Hydrogen

Hydrogen is a ubiquitous impurity that is present in most growth and processing environments, and is easily incorporated in materials. In semiconductors, interstitial hydrogen usually acts as an amphoteric impurity, that is, it behaves as a donor in p-type material and as an acceptor in n-type material [45, 46]. This implies that hydrogen counteracts the prevailing conductivity, and will have a tendency to form complexes with dopant impurities [47]. In germanium, however, hydrogen exhibits a less usual behavior where it is always negatively charged [48, 49]. The reason for this behavior is linked to the fairly high position of the germanium VBM on an absolute energy scale [50]. Combined with the fact that the electronic defect level associated with interstitial hydrogen is approximately constant on an absolute energy scale, this explains why hydrogen in silicon is amphoteric while in germanium hydrogen is exclusively an acceptor. This behavior has important consequences for hydrogen's ability to passivate defects in germanium, as will be discussed in Section 1.4.4.

1.4
Intrinsic Defects

We have already mentioned that native defects can interact with impurity atoms and determine their diffusivity. In addition, native point defects can be electrically active and introduce defect levels within the band gap. Such energy levels can degrade device performance, as will be discussed in Section 1.4.4. In bulk germanium, native defects can take the form of vacancies (missing atoms) or interstitials (extra atoms). At interfaces, native defects can be characterized by a lack of consistent bonding across the interface; such defects are referred to as DBs.

1.4.1
Vacancies

1.4.1.1 Electronic Structure

When a vacancy is created in germanium, an atom is removed and four bonds are broken. The remaining DBs can be represented as sp^3 orbitals (Figure 1.2). The interaction of these orbitals produces a symmetric state (commonly referred to as a_1) and three degenerate states (commonly referred to as t_2). Depending on the occupancy of these states (as determined by the charge state of the vacancy), the degeneracy of the t_2 states can be split by Jahn–Teller distortions. These t_2 states can also be split by strain or the presence of another defect or impurity atom nearby. An assessment of the stability of different charge states requires a discussion of the formation energy of the vacancy.

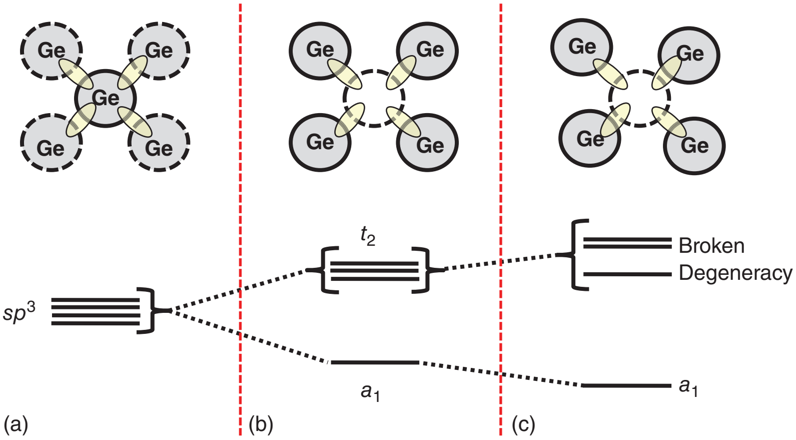

Figure 1.2 Electronic structure of the vacancy in germanium. (a) sp^3 bonding orbitals in germanium. (b) Symmetric a_1 and degenerate t_2 defect states for the vacancy in germanium. (c) Symmetry breaking can split the t_2 states due to strain, Jahn–Teller distortion, or nearby defects.

1.4.1.2 Formation Energy

The formation energy is a key quantity for characterizing defects in solids. In the dilute regime and assuming thermal equilibrium, the formation energy (E^f) of a defect is related to its concentration through a Boltzmann relation [24]:

$$C = N_0 \ e^{-E^f/k_B T}, \tag{1.1}$$

where N_0 is the number of sites the defect can incorporate on, including the number of possible configurations per site, k_B is the Boltzmann constant, and T is the temperature. For a vacancy in charge state $q(V_{\mathrm{Ge}}^q)$, the formation energy is defined as follows [24]:

$$E^f[V_{\mathrm{Ge}}^q] = E_{\mathrm{tot}}[\mathrm{Ge} : V_{\mathrm{Ge}}^q] - E_{\mathrm{tot}}[\mathrm{Ge} : \mathrm{bulk}] + \mu_{\mathrm{Ge}} + q\varepsilon_F. \tag{1.2}$$

The E_{tot} terms are the total energies of the germanium crystal with and without the defect. For the defect, a supercell geometry is used. Note that inclusion of spin polarization is essential to ensure correct occupation of the defect states. μ_{Ge} is the chemical potential, representing the energy of the reservoir in which the germanium atom that was removed from the solid was placed. In the case of an elemental solid such as germanium, this is simply the energy per atom of a bulk germanium crystal. Sometimes this is presented as placing the germanium atom that was removed on the surface of the material; this increases the number of bulk atoms by one, leading to the same conclusion that the reference energy is equivalent to that of a bulk germanium atom.

When the vacancy is in charge state q, q electrons have been removed from the defect, and these electrons have been placed in a reservoir with energy ε_F, that is, the electron chemical potential or (in semiconductor language) the Fermi level. Typically, ε_F is referenced to the bulk VBM. The Fermi level in Eq. (1.2) is a

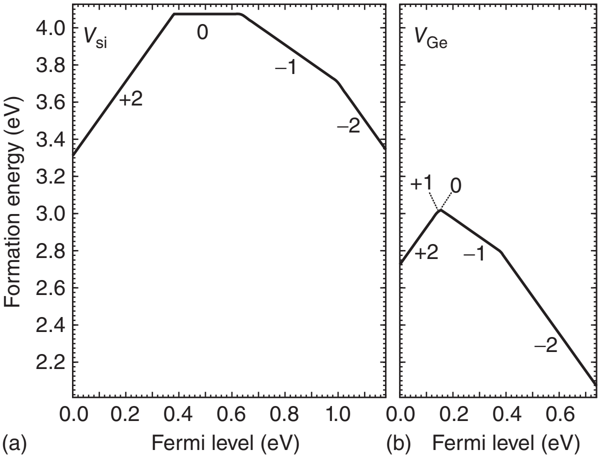

Figure 1.3 Formation energy of vacancies in silicon (a) and in germanium (b) as calculated with hybrid density functional theory [51]. Only the lowest energy charge state is shown for each value of the Fermi level.

variable. In practice, the Fermi level is of course fixed to a value that is determined by local charge neutrality, taking into account all point defects and all impurities (in all possible charge states) that are present in the material. However, we will see that it is instructive to examine the formation energy of the defect as a function of ε_F, allowing us, for instance, to examine what would happen in p-type (ε_F close to the VBM) versus n-type material (ε_F close to the CBM).

We, therefore, plot the formation energy as a function of ε_F, as illustrated in Figure 1.3 for both Si and Ge. The values shown here were obtained with the hybrid density functional technique described in Section 1.2.2, using the HSE functional. For calculational details we refer to Ref. [51]. For a given value of the Fermi level, only the lowest energy charge state is shown, and the slope of the line segment corresponds to the charge of the defect. We note that the concentration of higher energy charge states is exponentially attenuated (Eq. (1.1)).

Figure 1.3 shows that germanium vacancies have a significantly smaller formation energy than silicon vacancies. Consequences, particularly for diffusion, will be discussed in Section 1.4.1.5.

1.4.1.3 **Defect Levels**

The kinks in the curve indicate transitions between different charge states of the defect. The Fermi-level positions at which these occur determine the so-called charge-state transition levels (q/q'), which can be derived from the calculated formation energies:

$$(q/q') = -\frac{E^f(\mathrm{D}^q; \varepsilon_F = 0) - E^f(\mathrm{D}^{q'}; \varepsilon_F = 0)}{q - q'} , \tag{1.3}$$

Table 1.4 Charge-state transition levels associated with the vacancies in silicon and germanium as calculated with hybrid density functional theory [51].

Transition Level	Silicon (eV)	Germanium (eV)
$(+2/+1)$	–	0.14
$(+1/0)$	–	0.15
$(+2/0)$	0.38	–
$(0/-1)$	0.63	0.16
$(-1/-2)$	1.00	0.38

where $E^f(\mathrm{D}^q; \varepsilon_F = 0)$ is the formation energy of the defect D in charge state q when the Fermi level is at the VBM. For $\varepsilon_F < (q/q')$, the defect is stable in charge state q, while for $\varepsilon_F > (q/q')$, the defect is stable in charge q'. These transition levels are also sometimes referred to as thermodynamic transition levels, and can be probed using experimental techniques such as DLTS, in which the final charge state is able to fully relax to its corresponding equilibrium atomic configuration after the charge-state transition.

Table 1.4 lists the charge-state transition levels for the vacancies in germanium and silicon. Table 1.4 and Figure 1.3 show that the $(+2/+1)$, $(+1/0)$, and $(0/-1)$ charge-state transition levels in germanium are very close in energy. PACS measurements have found the $(0/-1)$ transition level to be located at 0.2 ± 0.04 eV above the germanium VBM [52, 53], in good agreement with the result in Table 1.4. The $(-1/-2)$ level is calculated to be 0.38 eV above the VBM in germanium. A vacancy-related charge-state transition level at 0.33 eV has been detected with DLTS [54].

Physical insight into the formation of the +2, +1, 0, and −1 charge states and the corresponding transition levels can be obtained by considering the single-particle states introduced in Section 1.4.1.1. We illustrate these single-particle states in Figure 1.4. In the neutral charge state of the vacancy, four electrons (one from each germanium sp^3 orbital) are available to fill the vacancy-induced single-particle KS states. Two electrons go into the a_1 state (below the VBM) and two are left to occupy the spin-up channel of the t_2 states, leading to a spin-1 configuration. The +1 charge state of the vacancy is obtained by removing one electron from the t_2 states, leading to a configuration with spin 1/2. Removing a second electron leads to the +2 charge state and a spin-0 configuration. The a_1 states, which are well below the VBM, always remain occupied, and hence the +2 charge state is the lowest achievable charge state of the vacancy. Upon adding one additional electron to obtain the −1 charge state, there are 5 electrons: 2 in the a_1 state, and 3 in the spin-up channel of the t_2 states, which are thus occupied with one electron each. This leads to a spin-3/2 configuration. We thus see that starting from +2, the +1, 0, and −1 charge states are obtained by adding one, two, or three electrons to the spin-majority channel of the t_2 states. These electrons go into different orbitals, and apparently inter-orbital repulsion is quite weak, explaining why the $(+2/+1)$,

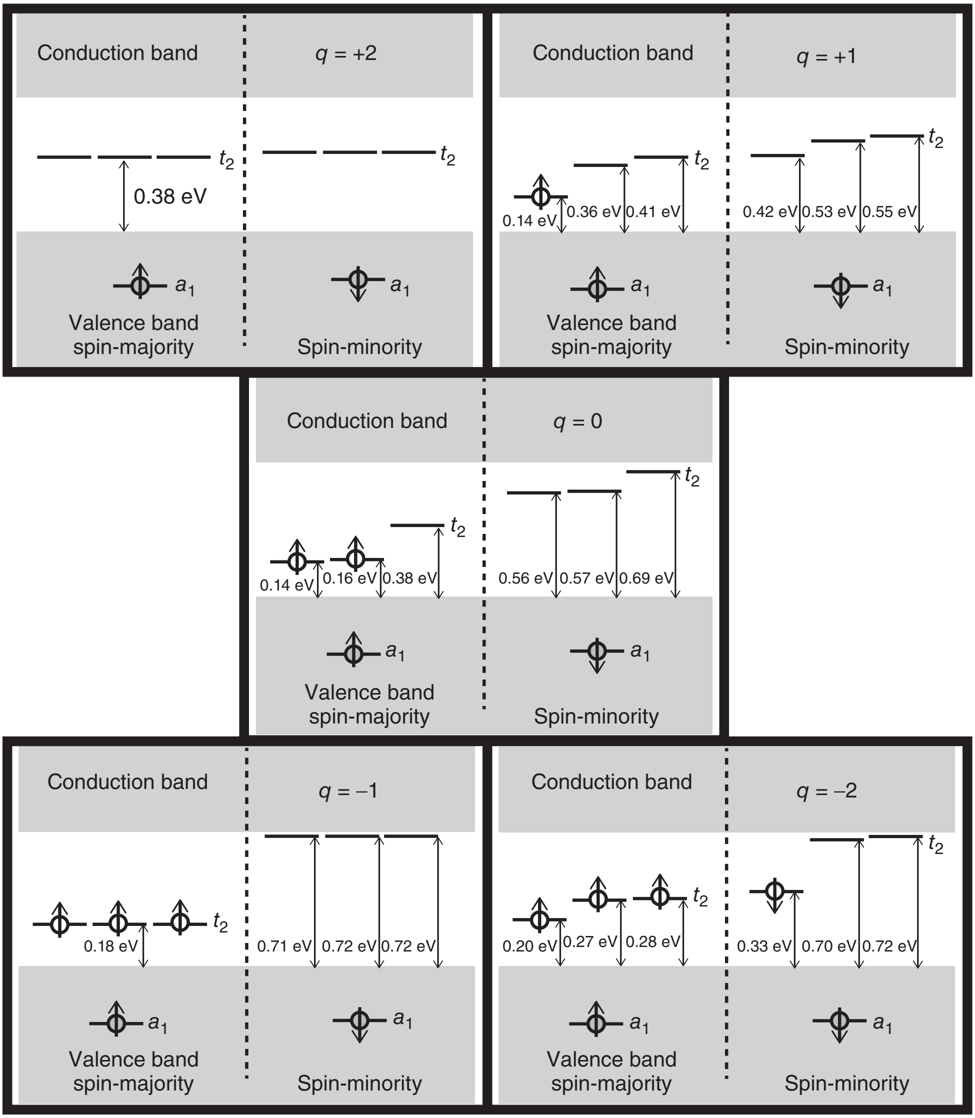

Figure 1.4 Kohn–Sham states for the +2 to −2 charge states of the vacancy in germanium. These results were obtained through spin-polarized hybrid density functional theory calculations [51].

(+1/0), and (0/ − 1) charge-state transition levels are very close together in energy, as seen in Table 1.4.

To obtain the −2 charge state, however, an electron must now be added to the spin-minority channel associated with the t_2 states. This now causes intra-orbital electron–electron repulsion (apparently much stronger than inter-orbital repulsion) between the two electrons in the t_2 state that is doubly occupied; a significant rearrangement of the single-particle states occurs and explains the large separation between the $(0/-1)$ and $(-1/-2)$ charge-state transition levels, as seen in Table 1.4).

The results shown in Figure 1.3 and Table 1.4 are in broad agreement with other density functional calculations for vacancies in germanium reported in the literature [35, 36, 55]. The discrepancies that do occur can be mainly attributed to the different approximations made within the DFT framework. In the study by Fazzio *et al.* [55] modifications were made to the germanium pseudopotential, while Śpiewak *et al.* [35] employed LDA+U and Tahini *et al.* [36] used GGA+U. In addition, the studies by Fazzio *et al.* [55] and Tahini *et al.*[36] did not consider spin polarization, which is essential to obtain a correct occupation of single-particle states.

1.4.1.4 Comparison with Silicon

Figure 1.3 shows that the +1 charge state is not stable in silicon, while the +1 charge state of the vacancy in germanium is stable over a small but finite range of Fermi levels. The calculations for silicon [51] show that the +1 charge state is never thermodynamically stable. Such a situation, where the stable charge state as a function of Fermi level jumps from +2 to 0, is referred to as a negative$-U$ transition [56]. Experimentally, the fact that the +1 charge state of the silicon vacancy is not stable has indeed been observed using DLTS [57].

The relative spacing of the charge-state transition levels of the vacancy is very different in silicon and germanium (Figure 1.3). The difference can be mainly attributed to the different behavior of the neutral charge state. In germanium, the atomic structures of the +2, +1, 0, and −1 charge states are quite similar, that is, the atomic relaxations do not drastically change as electrons are added to the t_2 spin-up states. But in silicon, the neutral charge state exhibits distinctly larger relaxations, indicative of extensive rebonding (probably induced by silicon's smaller lattice constant) and resulting in a lowering of the energy of this charge state relative to the other charge states. This Jahn–Teller distortion lowers the two occupied t_2 eigenvalues with respect to the unoccupied one and is responsible for the much larger spacing of the $(+1/0)$ and $(0/-1)$ transition levels in silicon compared to germanium.

1.4.1.5 Diffusion

Self-diffusion in germanium is known to be largely governed by vacancies [1, 4, 5]. The diffusion activation energy is the sum of formation energy and migration barrier. A migration barrier of 0.1 eV was calculated for the vacancy in germanium [58]. The formation energy is a function of Fermi level. For modest doping levels (below $\sim 5\times10^{18}$ cm^{-3}) the material is close to intrinsic at the temperatures of interest for diffusion, and under those conditions the vacancy will likely be in a −1 charge state, with a formation energy of ∼ 2.9 eV (Figure 1.3). Combined with the migration barrier, this leads to an activation energy for self-diffusion of 3.0 eV, in remarkable agreement with the experimental values of 3.1 eV [1].

Assuming that vacancies are also a major contributor to self-diffusion in silicon, the same exercise leads to a migration barrier of 0.5 eV [59] and a formation energy of 4.1 eV for the neutral charge state (Figure 1.3), resulting in an activation energy of 4.6 eV—again in good agreement with the experimental value of 4.8 eV [60].

We note that that the value of the formation energy of the vacancy depends on the Fermi level (Figure 1.3), and therefore doping may impact self-diffusion, particularly at high doping levels. This has indeed been observed experimentally [61].

1.4.2
Self-Interstitials

Self-interstitials are formed when extra atoms are added to the crystal. Self-interstitials can exist in a variety of atomic configurations, illustrated in Figure 1.5.

The split interstitial is formed by placing two atoms on a single lattice site. The orientation of these two atoms defines the type of split interstitial. In both silicon and germanium, the <110> orientation (illustrated in Figure 1.5a) is the lowest in energy for stable charge states of the split-interstitial [62–65]. The hexagonal interstitial is formed by placing a germanium atom on a sixfold coordinated interstitial site, while the tetrahedral interstitial is located on a fourfold-coordinated site. Intermediate structures can be formed by placing an interstitial atom at a

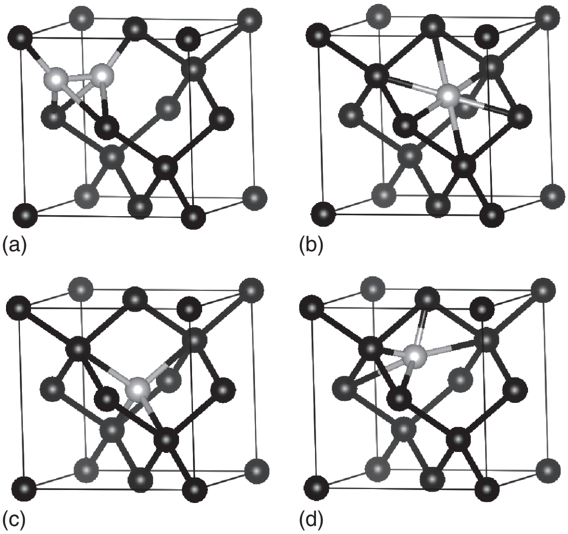

Figure 1.5 Atomic configuration for various types of self-interstitial defects in germanium. The types are defined as: (a) split interstitial, (b) hexagonal interstitial, (c) tetrahedral interstitial, and (d) open cage structure formed by a bond-center interstitial atom relaxing outward toward the hexagonal site (distorted hexagonal structure). Black atoms indicate bulk-like atoms. Gray atoms indicate the interstitial atom(s).

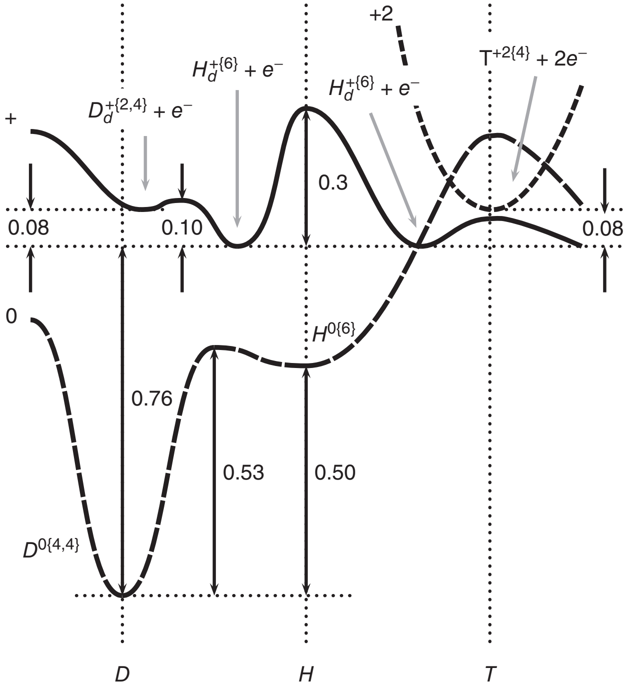

Figure 1.6 Configuration-coordinate diagram for the self-interstitial in germanium. *D* denotes the split-interstitial, *H* the hexagonal interstitial, and *T* the tetrahedral interstitial. Figure courtesy of Ref. [63].

bond-center location and then allowing the structure to relax toward the tetrahedral or hexagonal configuration [66].

Because the interstitial can exist in different atomic configurations, it is possible for the lowest-energy atomic configuration of one charge state to be different from that in a different charge state. First-principles calculations based on DFT-LDA combined with nonlinear core corrections for the germanium *d* states [63] indicated that the neutral charge state is stable in the split-interstitial configuration, while the +2 charge state is stable in the tetrahedral configuration. The +1 charge state is most stable in an open cage structure similarly to Figure 1.5d (distorted hexagonal configuration) [63, 66].

Because of this stability in different atomic configurations, it is important to understand the barriers associated with the various interstitial configurational transformations. Figure 1.6 illustrates these barriers, as well as the lowest energy configurations for the 0, +1, and +2 charge states. We see that the barriers associated with metastable states for the neutral and +1 charge states are very small, indicating that it is unlikely that interstitials will become trapped in metastable states.

First-principles calculations based on DFT-LDA consistently find the (+1/0) charge-state transition level to be very close to the VBM [64, 65]. Experimentally, PACS data suggests that the self-interstitial produces a transition level in the vicinity of the CBM [52, 53]. The origin of this particular transition has been debated [64, 65], but the most likely assignment is the $(0/-1)$ transition. We note that calculations for self-interstitials to date have been performed only with DFT-LDA [64, 65], making conclusive assignments difficult due to the band-gap problem.

In germanium, the self-interstitial is a less important defect than the vacancy because of its significantly higher formation energy [4, 5]. Dopant diffusion in germanium is predominantly mediated by vacancies [4, 5].

1.4.3
Dangling Bonds

1.4.3.1 Electronic Levels

Vacancies and self-interstitials are point defects that occur within the bulk of a germanium crystal. At an interface with another semiconductor or insulator, deviations from perfect coordination may occur, leading to DBs. Figure 1.7 illustrates a schematic atomic configuration for a DB at a germanium/germanium-oxide interface.

A number of first-principles calculations have been performed for DBs in silicon [68, 69] and germanium [48, 51, 69]. Figure 1.8 displays the results for DB defect levels from Ref. [51], again comparing silicon and germanium.

Calculations for DBs in silicon place the $(+/0)$ level at an energy of about 0.1–0.2 eV above the VBM, and the $(0/-)$ level at about 0.6–0.8 eV, indicating that the neutral DB would be stable over quite a large range of Fermi levels within the band gap [51, 69] (Table 1.5). This agrees with EPR experiments [71–73] that probe the neutral charge state of the DB of an MOS capacitor, finding that the neutral charge state is stable over a 0.5 eV range within the silicon band gap [71].

Calculations for DBs in germanium lead to results for the DB levels that agree to within about 0.2 eV [51, 69], with the defect levels occurring near the germanium

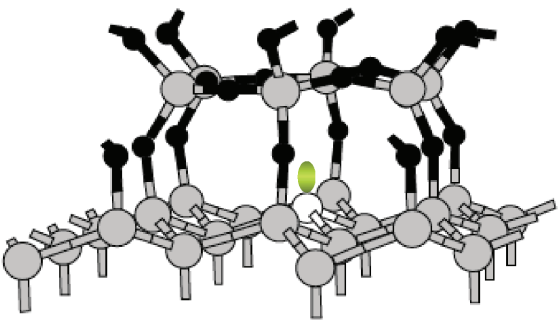

Figure 1.7 Schematic representation of a dangling bond at a germanium/germanium-oxide interface. Gray atoms represent germanium, black atoms oxygen, and the white atom the germanium atom with the DB. Figure courtesy of Ref. [67].

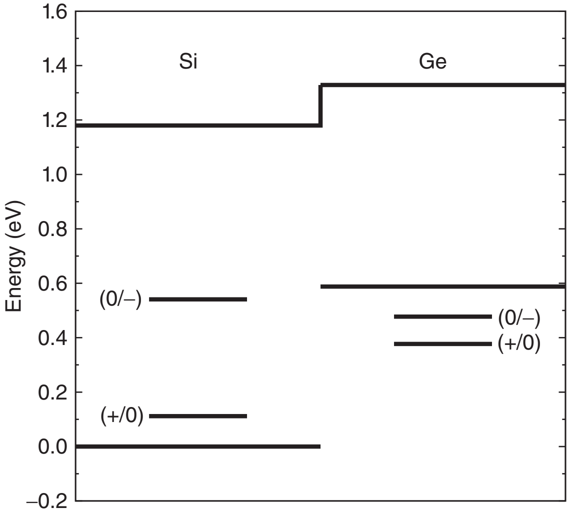

Figure 1.8 Charge-state transition levels for dangling bonds in silicon and germanium as calculated with hybrid density functional theory [51]. The connected bottom lines indicate the VBM for silicon and germanium, while the connected top lines indicate the CBM for these materials. The alignment of the band structures is based on the calculated valence-band offset of 0.6 eV [70]. The short lines indicate the charge-state transition levels associated with the dangling bonds [51].

Table 1.5 Charge-state transition levels associated with the dangling bonds in silicon and germanium as calculated with hybrid density functional theory [51].

Transition Level	Silicon (eV)	Germanium (eV)
$(0/-1)$	0.10	−0.11
$(+1/0)$	0.55	−0.21

VBM. Some of the calculations place the (0/−) level of the DB below the VBM [48, 51], while others place it just above the VBM [69]. Although the quantitative difference is quite small, this leads to qualitatively different results: in one case, the DB can only be stable in a negative charge state (and thus not be observable by ESR, which requires a neutral charge state), while in the other, different charge states are in principle possible—although the authors of Ref. [69] argued that the concentration of neutral DBs would be small. ESR experiments have been unsuccessful at detecting DBs at germanium/oxide interfaces [74], indicating that the concentration of neutral DBs is undetectably small.

Additional experimental information is provided by ESR studies of $Si_{1-x}Ge_x/SiO_2$ interfaces [75, 76], by analyzing the interfacial ESR signal as a function of the germanium concentration (x). The results were used to provide an estimate of where the germanium DB defect level would lie if referenced to the silicon band gap, resulting in a value 0.35 ± 0.10 eV above the silicon VBM [76]. If we use the data in Figure 1.8 and assume that the germanium DB level remains constant on an absolute energy scale as the alloy concentration is changed—a reasonable assumption for a highly localized state such as the DB—we can use the valence-band offset between silicon and germanium (0.6 eV [70]) to estimate the position of the germanium DB level in pure silicon; this estimate leads to a value for the germanium DB $(0/-1)$ level of 0.49 eV above the Si VBM, in reasonable agreement with the experimental determination. If anything, experimental results point to an even lower position of the germanium DB than what is depicted in Figure 1.8.

Therefore, by combining existing experimental data with current state-of-the-art *ab initio* calculations, we obtain a complete and consistent picture of the DB in germanium. Comparing these results with those for the silicon DB (as presented in Figure 1.8), we expect DBs to behave very differently in germanium-based devices than they do in silicon-based devices. In Section 1.4.4 we discuss this in detail.

1.4.4
Impact on Devices

Compared with silicon, germanium CMOS devices still lag in performance. *p*-channel MOSFETs show acceptable performance but exhibit an undesirable positive threshold voltage shift [77]. *n*-channel MOSFETs suffer from low channel mobilities and on-state currents [78–80]. These problems are likely caused by the presence of defects, such as germanium DBs, near the semiconductor/dielectric interface. In Section 1.4.3.1 we discussed that the levels of the DB in germanium are likely to be below the VBM, causing it to always be negatively charged. DB defects near an interface will therefore give rise to negative fixed charge, creating serious problems for devices that rely on the formation of an electron channel (such as *n*-channel MOSFETs) [81]. Even for *p*-channel devices, such fixed charge will induce undesirable carrier scattering, as well as a positive threshold voltage shift, which has also been experimentally observed [77].

DBs are known to also occur at silicon/oxide interfaces. As illustrated in Figure 1.8), silicon DBs induce defect levels within the silicon band gap, which, in principle, also act as carrier traps in MOS devices. In silicon, hydrogen is very effective at passivating interfacial DB defects [82]. Hydrogen can bind to the silicon DB, forming an Si–H bond that has no defect levels in the band gap.

However, as discussed in Section 1.3.2, hydrogen behaves very differently in germanium compared to silicon. In silicon, hydrogen is an amphoteric impurity, but in germanium, hydrogen acts exclusively as an acceptor and is thus always negatively charged [48, 49]. Hydrogen interstitials will thus be electrostatically repelled from DBs in germanium, and will not effectively passivate DB defects. This is consistent with experimental observations showing that hydrogenation is ineffective in reducing interface-state densities at germanium/oxide interfaces [74]. Given the inability of hydrogen to passivate DB defects, alternative passivation strategies will need to be explored for germanium.

1.5
Summary

We have discussed the atomic and electronic structure of dopant impurities, point defects, DBs, and hydrogen in germanium, along the way comparing with silicon. We showed how results from first-principles calculations can help in interpreting experimental results and aid in developing a complete understanding of defects. Specifically, we discussed the origin of defect levels introduced by germanium vacancies, comparing to silicon. For the germanium interstitial, we illustrated the various configurations and charge states for which it can be stable. DBs as well as hydrogen exhibit qualitatively different behavior in silicon versus germanium. This leads to a number of problems for germanium-based devices, and the need for novel passivation schemes.

References

1. Hüger, E., Tietze, U., Lott, D., Bracht, H., Bougeard, D., Haller, E.E., and Schmidt, H. (2008) Self-diffusion in germanium isotope multilayers at low temperatures. *Appl. Phys. Lett.*, **93** (16), 162104, doi: 10.1063/1.3002294.
2. Bracht, H. and Brotzmann, S. (2006) Atomic transport in germanium and the mechanism of arsenic diffusion. *Mater. Sci. Semicond. Process.*, **9**, 471–476.
3. Nichols, C.S., Van de Walle, C.G., and Pantelides, S.T. (1989) Mechanisms of equilibrium and nonequilibrium diffusion of dopants in silicon. *Phys. Rev. Lett.*, **62**, 1049–1052, doi: 10.1103/PhysRevLett.62.1049.
4. Chroneos, A., Bracht, H., Grimes, R.W., and Uberuaga, B.P. (2008) Vacancy-mediated dopant diffusion activation enthalpies for germanium. *Appl. Phys. Lett.*, **92** (17), 172103, doi: 10.1063/1.2918842.
5. Brotzmann, S. and Bracht, H. (2008) Intrinsic and extrinsic diffusion of phosphorus, arsenic, and antimony in germanium. *J. Appl. Phys.*, **103** (3), 033 508, doi: http://dx.doi.org/10.1063/1.2837103.
6. Dargys, A. and Kundrotas, J. (1994) *Handbook on Physical Properties of Ge, Si, GaAs and InP*, Vol. 1, Science and Encyclopedia Publishers, Vilnius, LT, p. 1.
7. Schroder, D. (2006) *Semiconductor Material and Device Characterization*, Vol. 1, John Wiley & Sons, Inc., p. 1.
8. Sze, S.M. (1981) *Physics of Semiconductor Devices*, Vol. 1, John Wiley & Sons, Inc., Hoboken, NJ, p. 1.
9. Watkins, G.D. (1999) Identification of defects in semiconductors, in *Semiconductors and Semimetals*, Vol. 51A (ed. M. Stavola), Academic Press, San Diego, CA, p. 1.
10. Kennedy, T.A. and Glaser, E.R. (1999) Identification of defects in semiconductors, in *Semiconductors and Semimetals*, Vol. 51A (ed. M. Stavola), Academic Press, San Diego, CA, p. 1.
11. Van de Walle, C.G. (1990) Structural identification of hydrogen and muonium centers in silicon: first-principles calculations of hyperfine parameters. *Phys. Rev. Lett.*, **64**, 669–672, doi: 10.1103/PhysRevLett.64.669.
12. Van de Walle, C.G. and Blöchl, P.E. (1993) First-principles calculations of hyperfine parameters. *Phys. Rev. B*, **47**, 4244–4255, doi: 10.1103/PhysRevB.47.4244.
13. McCluskey, M.D. (2000) Local vibrational modes of impurities in semiconductors. *J. Appl. Phys.*, **87** (8), 3593–3617, doi: 10.1063/1.372453.
14. Limpijumnong, S., Northrup, J.E., and Van de Walle, C.G. (2003) Identification of hydrogen configurations in *p*-type

GaN through first-principles calculations of vibrational frequencies. *Phys. Rev. B*, **68**, 075 206, doi: 10.1103/PhysRevB.68.075206.

15. Puska, M.J. and Nieminen, R.M. (1994) Theory of positrons in solids and on solid surfaces. *Rev. Mod. Phys.*, **66**, 841–897, doi: 10.1103/RevModPhys.66.841.
16. Look, D.C. (1992) Electrical characterization of GaAs materials and devices, *Design and Measurement in Electronic Engineering*, Vol. 1, John Wiley & Sons, Inc., p. 1.
17. Mooney, P.M. (1999) Identification of defects in semiconductors, in Semiconductors and Semimetals, Vol. 51B (ed. M. Stavola), Academic Press, San Diego, CA, p. 93.
18. Davies, G. (1999) Identification of defects in semiconductors, in *Semiconductors and Semimetals*, Vol. 51B (ed. M. Stavola), Academic Press, San Diego, CA, p. 1.
19. Zacate, M.O. and Jaeger, H. (2011) Perturbed angular correlation spectroscopy: a tool for the study of defects and diffusion at the atomic scale. *Defect Diffus. Forum*, **311**, 3–38, doi: 10.4028/www.scientific.net/DDF.311.3.
20. Austin, J.C., Price, K., Patnaik, B.K., and Swanson, M.L. (1996) Perturbed-angular-correlation measurements of trivalent indium defects in silver bromide. *J. Phys. Condens. Matter*, **8**, 2679–2694, doi:10.1088/0953-8984/8/15/017.
21. Hohenberg, P. and Kohn, W. (1964) Inhomogeneous electron gas. *Phys. Rev.*, **136** (3B), B864–B871, doi: 10.1103/PhysRev.136.B864.
22. Kohn, W. and Sham, L.J. (1965) Self-consistent equations including exchange and correlation effects. *Phys. Rev.*, **140** (4A), A1133–A1138, doi: 10.1103/PhysRev.140.A1133.
23. Payne, M.C., Teter, M.P., Allan, D.C., Arias, T.A., and Joannopoulos, J.D. (1992) Iterative minimization techniques for ab initio total-energy calculations: molecular dynamics and conjugate gradients. *Rev. Mod. Phys.*, **64** (4), 1045–1097, doi: 10.1103/RevModPhys.64.1045.
24. Van de Walle, C.G. and Neugebauer, J. (2004) First-principles calculations for defects and impurities: applications to III-nitrides. *J. Appl. Phys.*, **95** (8), 3851–3879, doi: 10.1063/1.1682673.
25. Langreth, D.C. and Perdew, J.P. (1980) Theory of nonuniform electronic systems: analysis of the gradient approximation and a generalization that works. *Phys. Rev. B*, **21**, 5469–5493, doi: 10.1103/PhysRevB.21.5469.
26. Perdew, J.P. and Yue, W. (1986) Accurate and simple density functional for the electronic exchange energy: generalized gradient approximation. *Phys. Rev. B*, **33** (12), 8800–8802, doi: 10.1103/PhysRevB.33.8800.
27. Ceperley, D.M. and Alder, B.J. (1980) Ground state of the electron gas by a stochastic method. *Phys. Rev. Lett.*, **45** (7), 566–569, doi: 10.1103/PhysRevLett.45.566.
28. Perdew, J.P. and Zunger, A. (1981) Self-interaction correction to density-functional approximations for many-electron systems. *Phys. Rev. B*, **23** (10), 5048–5079, doi: 10.1103/PhysRevB.23.5048.
29. Aulbur, W.G., Jönsson, L., and Wilkins, J.W. (1999) Quasiparticle calculations in solids. *Solid State Phys.*, **54**, 1–218, doi: 10.1016/S0081-1947(08)60248-9.
30. Hedin, L. (1965) New method for calculating the one-particle Green's function with application to the electron-gas problem. *Phys. Rev.*, **139**, A796–A823, doi: 10.1103/PhysRev.139.A796.
31. Sánchez-Friera, P. and Godby, R.W. (2000) Efficient total energy calculations from self-energy models. *Phys. Rev. Lett.*, **85**, 5611–5614, doi: 10.1103/PhysRevLett.85.5611.
32. Bechstedt, F., Fuchs, F., and Kresse, G. (2009) Ab-initio theory of semiconductor band structures: new developments and progress. *Phys. Status Solidi B*, **246**, 1877–1892, doi: 10.1002/pssb.200945074.
33. Zhang, S.B., Wei, S.H., and Zunger, A. (2001) Intrinsic n-type versus p-type doping asymmetry and the defect physics of ZnO. *Phys. Rev. B*, **63**, 075 205, doi: 10.1103/PhysRevB.63.075205.

34. Segev, D., Janotti, A., and Van de Walle, C.G. (2007) Self-consistent band-gap corrections in density functional theory using modified pseudopotentials. *Phys. Rev. B*, **75** (3), 035 201, doi: 10.1103/PhysRevB.75.035201.

35. Śpiewak, P., Vanhellemont, J., Sueoka, K., Kurzydłowski, K.J., and Romandic, I. (2008) First principles calculations of the formation energy and deep levels associated with the neutral and charged vacancy in germanium. *J. Appl. Phys.*, **103** (8), 086103, doi: 10.1063/1.2907730.

36. Tahini, H., Chroneos, A., Grimes, R.W., Schwingenschlögl, U., and Bracht, H. (2011) Diffusion of *E* centers in germanium predicted using GGA+U approach. *Appl. Phys. Lett.*, **99** (7), 072112, doi: 10.1063/1.3625939.

37. Perdew, J.P., Ernzerhof, M., and Burke, K. (1996) Rationale for mixing exact exchange with density functional approximations. *J. Chem. Phys.*, **105** (22), 9982–9985, doi: 10.1063/1.472933.

38. Ernzerhof, M., Perdew, J.P., and Burke, K. (1997) Coupling-constant dependence of atomization energies. *Int. J. Quantum Chem.*, **64** (3), 285–295, doi: 10.1002/(SICI)1097-461X(1997)64:3<285::AID-QUA2>3.0.CO;2-S.

39. Ernzerhof, M. and Scuseria, G.E. (1999) Assessment of the Perdew–Burke–Ernzerhof exchange-correlation functional. *J. Chem. Phys.*, **110** (11), 5029–5036, doi: 10.1063/1.478401.

40. Adamo, C. and Barone, V. (1999) Toward reliable density functional methods without adjustable parameters: the PBE0 model. *J. Chem. Phys.*, **110** (13), 6158–6170, doi: 10.1063/1.478522.

41. Heyd, J., Scuseria, G.E., and Ernzerhof, M. (2003) Hybrid functionals based on a screened coulomb potential. *J. Chem. Phys.*, **118** (18), 8207–8215, doi: 10.1063/1.1564060.

42. Heyd, J., Scuseria, G.E., and Ernzerhof, M. (2006) Erratum: "Hybrid functionals based on a screened coulomb potential" [(2003) J. Chem. Phys., 118, 8207]. *J. Chem. Phys.*, **124** (21), 219906, doi: 10.1063/1.2204597.

43. Trumbore, F.A. (1960) Solid solubilities of impuritiy elements in germanium and silicon. *Bell Tech. J.*, **39**, 205–233.

44. Bracht, H. (2000) Diffusion mechanisms and intrinsic point-defect properties in silicon. *MRS Bull.*, **25** (6), 22–27.

45. Van de Walle, C.G. and Neugebauer, J. (2006) Hydrogen in semiconductors. *Annu. Rev. Mater. Res.*, **36** (1), 179–198, doi: 10.1146/annurev.matsci.36.010705.155428.

46. Herring, C., Johnson, N.M., and Van de Walle, C.G. (2001) Energy levels of isolated interstitial hydrogen in silicon. *Phys. Rev. B*, **64**, 125 209, doi: 10.1103/PhysRevB.64.125209.

47. Denteneer, P.J.H., Van de Walle, C.G., and Pantelides, S.T. (1989) Structure and properties of hydrogen-impurity pairs in elemental semiconductors. *Phys. Rev. Lett.*, **62**, 1884–1887, doi: 10.1103/PhysRevLett.62.1884.

48. Weber, J.R., Janotti, A., Rinke, P., and Van de Walle, C.G. (2007) Dangling-bond defects and hydrogen passivation in germanium. *Appl. Phys. Lett.*, **91** (14), 142101, doi: 10.1063/1.2793184.

49. Van de Walle, C.G., Weber, J.R., and Janotti, A. (2008) Role of hydrogen at germanium/dielectric interfaces. *Thin Solid Films*, **517** (1), 144 – 147, doi: 10.1016/j.tsf.2008.08.071. 5th International Conference on Silicon Epitaxy and Heterostructures (ICSI-5).

50. Van de Walle, C.G. and Neugebauer, J. (2003) Universal alignment of hydrogen levels in semiconductors, insulators and solutions. *Nature*, **423** (6940), 626–628.

51. Weber, J.R., Janotti, A., and Van de Walle, C.G. (2013) Dangling bonds and vacancies in germanium. *Phys. Rev. B*, **87**, 035203-1–035203-9.

52. Haesslein, H., Sielemann, R., and Zistl, C. (1998) Vacancies and self-interstitials in germanium observed by perturbed angular correlation spectroscopy. *Phys. Rev. Lett.*, **80** (12), 2626–2629, doi: 10.1103/PhysRevLett.80.2626.

53. Hasslein, H., Sielemann, R., and Zistl, C. (1997) Microscopic study of the vacancy and self-interstitial in Germanium by PAC, in *Defects in Semiconductors - ICDS-19, PTS 1-3, Materials Science Forum*, Vol. 258-2 (eds G. Davies and

M.H. Nazare), Transtec Publications Ltd, Brandrain 6, CH-8707, Zurich-Uetikon, pp. 59 – 64.

54. Zistl, C., Sielemann, R., Hasslein, H., Gall, S., Braunig, D., and Bollmann, J. (1997) DLTS combined with perturbed angular correlation (PAC) on radioactive In-111 atoms in Ge, in *Defects in Semiconductors - ICDS-19, PTS 1-3, Materials Science Forum*, Vol. 258-2 (eds G. Davies and M.H. Nazare) Transtec Publications Ltd, Brandrain 6, CH-8707, Zurich-Uetikon, Switzerland, pp. 53 – 58.

55. Fazzio, A., Janotti, A., da Silva, A.J.R., and Mota, R. (2000) Microscopic picture of the single vacancy in germanium. *Phys. Rev. B*, **61** (4), R2401 – R2404, doi: 10.1103/PhysRevB.61.R2401.

56. Anderson, P.W. (1975) Model for the electronic structure of amorphous semiconductors. *Phys. Rev. Lett.*, **34** (15), 953 – 955, doi: 10.1103/PhysRevLett.34.953.

57. Watkins, G.D. and Troxell, J.R. (1980) Negative-U properties for point defects in silicon. *Phys. Rev. Lett.*, **44** (9), 593 – 596, doi: 10.1103/PhysRevLett.44.593.

58. Pinto, H., Coutinho, J., Torres, V., Öberg, S., and Briddon, P. (2006) Formation energy and migration barrier of a Ge vacancy from ab initio studies. *Mater. Sci. Semicond. Process.*, **9** (4), 498 – 502, doi: 10.1016/j.mssp.2006.08.045. *Proceedings of Symposium TE-MRS 2006 Spring Meeting on Germanium based semiconductors from materials to devices.*

59. Watkins, G.D. (1997) Native defects and their interactions with impurities in silicon. *MRS Proc.*, **469**, doi: 10.1557/PROC-469-139.

60. Bracht, H., Haller, E.E., and Clark-Phelps, R. (1998) Silicon self-diffusion in isotope heterostructures. *Phys. Rev. Lett.*, **81**, 393 – 396, doi: 10.1103/PhysRevLett.81.393.

61. Werner, M., Mehrer, H., and Hochheimer, H.D. (1985) Effect of hydrostatic pressure, temperature, and doping on self-diffusion in germanium. *Phys. Rev. B*, **32**, 3930 – 3937, doi: 10.1103/PhysRevB.32.3930.

62. Leung, W.K., Needs, R.J., Rajagopal, G., Itoh, S., and Ihara, S. (1999) Calculations of silicon self-interstitial defects. *Phys. Rev. Lett.*, **83**, 2351 – 2354, doi: 10.1103/PhysRevLett.83.2351.

63. Carvalho, A., Jones, R., Janke, C., Goss, J.P., Briddon, P.R., Coutinho, J., and Öberg, S. (2007) Self-interstitial in germanium. *Phys. Rev. Lett.*, **99**, 175 502, doi: 10.1103/PhysRevLett.99.175502.

64. da Silva, A.J.R., Janotti, A., Fazzio, A., Baierle, R.J., and Mota, R. (2000) Self-interstitial defect in germanium. *Phys. Rev. B*, **62**, 9903 – 9906, doi: 10.1103/PhysRevB.62.9903.

65. Moreira, M.D., Miwa, R.H., and Venezuela, P. (2004) Electronic and structural properties of germanium self-interstitials. *Phys. Rev. B*, **70**, 115 215, doi: 10.1103/PhysRevB.70.115215.

66. Clark, S.J. and Ackland, G.J. (1997) Ab initio calculations of the self-interstitial in silicon. *Phys. Rev. B*, **56**, 47 – 50, doi: 10.1103/PhysRevB.56.47.

67. Stirling, A., Pasquarello, A., Charlier, J.C., and Car, R. (2000) Dangling bond defects at $\mathrm{Si-SiO_2}$ interfaces: atomic structure of the P_{b1} center. *Phys. Rev. Lett.*, **85**, 2773 – 2776, doi: 10.1103/PhysRevLett.85.2773.

68. Van de Walle, C.G. and Street, R.A. (1994) Structure, energetics, and dissociation of Si-H bonds at dangling bonds in silicon. *Phys. Rev. B*, **49** (20), 14766 – 14769, doi: 10.1103/PhysRevB.49.14766.

69. Broqvist, P., Alkauskas, A., and Pasquarello, A. (2008) Defect levels of dangling bonds in silicon and germanium through hybrid functionals. *Phys. Rev. B*, **78** (7), 075 203, doi: 10.1103/PhysRevB.78.075203.

70. Van de Walle, C.G. and Martin, R.M. (1986) Theoretical calculations of heterojunction discontinuities in the Si/Ge system. *Phys. Rev. B*, **34** (8), 5621 – 5634, doi: 10.1103/PhysRevB.34.5621.

71. Poindexter, E.H., Gerardi, G.J., Rueckel, M.E., Caplan, P.J., Johnson, N.M., and Biegelsen, D.K. (1984) Electronic traps and P_b centers at the $\mathrm{Si/SiO_2}$ interface: Band-gap energy distribution. *J. Appl. Phys.*, **56** (10), 2844 – 2849, doi: 10.1063/1.333819.

72. Stesmans, A. (1993) Relationship between stress and dangling bond generation at the (111)Si/SiO_2 interface. *Phys. Rev. Lett.*, **70** (11), 1723–1726, doi: 10.1103/PhysRevLett.70.1723.

73. Stesmans, A. (1996) Passivation of P_{b0} and P_{b1} interface defects in thermal (100) Si/SiO_2 with molecular hydrogen. *Appl. Phys. Lett.*, **68** (15), 2076–2078, doi: 10.1063/1.116308.

74. Afanas'ev, V.V., Fedorenko, Y.G., and Stesmans, A. (2005) Interface traps and dangling-bond defects in (100)Ge/HfO_2. *Appl. Phys. Lett.*, **87** (3), 032107, doi: 10.1063/1.1947372.

75. Stesmans, A., Somers, P., and Afanas'ev, V.V. (2004) Nontrigonal Ge dangling bond interface defect in condensation-grown (100)$Si_{1-x}Ge_x/SiO_2$. *Phys. Rev. B*, **79** (19), 195 301, doi: 10.1103/PhysRevB.79.195301.

76. Afanas'ev, V.V., Houssa, M., Stesmans, A., Souriau, L., Loo, R., and Meuris, M. (2009) Electronic properties of Ge dangling bond centers at $Si_{1-x}Ge_x/SiO_2$ interfaces. *Appl. Phys. Lett.*, **95** (22), 222106, doi: 10.1063/1.3266853.

77. Ritenour, A., Khakifirooz, A., Antoniadis, D.A., Lei, R.Z., Tsai, W., Dimoulas, A., Mavrou, G., and Panayiotatos, Y. (2006) Subnanometer-equivalent-oxide-thickness germanium *p*-metal-oxide-semiconductor field effect transistors fabricated using molecular-beam-deposited high-κ/metal gate stack. *Appl. Phys. Lett.*, **88** (13), 132107, doi: 10.1063/1.2189456.

78. Whang, S.J., Lee, S.J., Gao, F., Wu, N., Zhu, C.X., Pan, L.S., Tang, L.J., and Kwong, D.L. (2004) Germanium *p*- and *n*-MOSFETs fabricated with novel surface passivation (plasma-PH3 and thin AlN) and TaN/HfO_2 gate stack. 2004 Int'l Electron Devices Meeting (IEDM), Vol. 1, San Francisco, CA, December 2004, pp. 307–310, doi: 10.1109/IEDM.2004.1419140.

79. Shang, H., Lee, K.L., Kozlowski, P., D'Emic, C., Babich, I., Sikorski, E., Ieong, M., Wong, H.S., Guarini, K., and Haensch, W. (2004) Self-aligned *n*-channel germanium MOSFETs with a thin Ge oxynitride gate dielectric and tungsten gate. *IEEE Electron Device Lett.*, **25** (3), 135–137, doi: 10.1109/LED.2003.823060.

80. Bai, W., Lu, N., Ritenour, A., Lee, M., Antoniadis, D., and Kwong, D.L. (2006) Ge *n*-MOSFETs on lightly doped substrates with high-κ dielectric and TaN gate. *IEEE Electron Device Lett.*, **27** (3), 175–178, doi: 10.1109/LED.2006.870242.

81. Dimoulas, A., Tsipas, P., Sotiropoulos, A., and Evangelou, E.K. (2006) Fermi-level pinning and charge neutrality level in germanium. *Appl. Phys. Lett.*, **89** (25), 252110, doi: 10.1063/1.2410241.

82. Tuttle, B. and Van de Walle, C.G. (1999) Structure, energetics, and vibrational properties of Si-H bond dissocttiation in silicon. *Phys. Rev. B*, **59**, 12884–12889, doi: 10.1103/PhysRevB.59.12884.